

Tritium calibration of the LUX detector

D.S. Akerib,¹ H.M. Araújo,² X. Bai,³ A.J. Bailey,² J. Balajthy,⁴ E. Bernard,⁵ A. Bernstein,⁶ A. Bradley,¹ D. Byram,⁷ S.B. Cahn,⁵ M.C. Carmona-Benitez,⁸ C. Chan,⁹ J.J. Chapman,⁹ A.A. Chiller,⁷ C. Chiller,⁷ T. Coffey,¹ A. Currie,² L. de Viveiros,¹⁰ A. Dobi,⁴ J. Dobson,¹¹ E. Druszkiewicz,¹² B. Edwards,⁵ C.H. Faham,¹³ S. Fiorucci,⁹ C. Flores,¹⁴ R.J. Gaitskell,⁹ V.M. Gehman,¹³ C. Ghag,¹⁵ K.R. Gibson,¹ M.G.D. Gilchriese,¹³ C. Hall,⁴ S.A. Hertel,⁵ M. Horn,⁵ D.Q. Huang,⁹ M. Ihm,¹⁶ R.G. Jacobsen,¹⁶ K. Kazkaz,⁶ R. Knoche,⁴ N.A. Larsen,⁵ C. Lee,¹ A. Lindote,¹⁰ M.I. Lopes,¹⁰ D.C. Malling,⁹ R. Mannino,¹⁷ D.N. McKinsey,⁵ D.-M. Mei,⁷ J. Mock,¹⁴ M. Moongweluwun,¹² J. Morad,¹⁴ A.St.J. Murphy,¹¹ C. Nehr Korn,⁸ H. Nelson,⁸ F. Neves,¹⁰ R.A. Ott,¹⁴ M. Pangilinan,⁹ P.D. Parker,⁵ E.K. Pease,⁵ K. Pech,¹ P. Phelps,¹ L. Reichhart,¹⁵ T. Shutt,¹ C. Silva,¹⁰ V.N. Solovov,¹⁰ P. Sorensen,⁶ K. O'Sullivan,⁵ T.J. Sumner,² M. Szydagis,¹⁴ D. Taylor,¹⁸ B. Tennyson,⁵ D.R. Tiedt,³ M. Tripathi,¹⁴ S. Uvarov,¹⁴ J.R. Verbus,⁹ N. Walsh,¹⁴ R. Webb,¹⁷ J.T. White,¹⁷ M.S. Witherell,⁸ F.L.H. Wolfs,¹² M. Woods,¹⁴ and C. Zhang⁷

¹Case Western Reserve University, Dept. of Physics, 10900 Euclid Ave, Cleveland OH 44106, USA

²Imperial College London, High Energy Physics, Blackett Laboratory, London SW7 2BZ, UK

³South Dakota School of Mines and Technology, 501 East St Joseph St., Rapid City SD 57701, USA

⁴University of Maryland, Dept. of Physics, College Park MD 20742, USA

⁵Yale University, Dept. of Physics, 217 Prospect St., New Haven CT 06511, USA

⁶Lawrence Livermore National Laboratory, 7000 East Ave., Livermore CA 94551, USA

⁷University of South Dakota, Dept. of Physics, 414E Clark St., Vermillion SD 57069, USA

⁸University of California Santa Barbara, Dept. of Physics, Santa Barbara, CA, USA

⁹Brown University, Dept. of Physics, 182 Hope St., Providence RI 02912, USA

¹⁰LIP-Coimbra, Department of Physics, University of Coimbra, Rua Larga, 3004-516 Coimbra, Portugal

¹¹SUPA, School of Physics and Astronomy, University of Edinburgh, Edinburgh, EH9 3JZ, UK

¹²University of Rochester, Dept. of Physics and Astronomy, Rochester NY 14627, USA

¹³Lawrence Berkeley National Laboratory, 1 Cyclotron Rd., Berkeley, CA 94720, USA

¹⁴University of California Davis, Dept. of Physics, One Shields Ave., Davis CA 95616, USA

¹⁵Department of Physics and Astronomy, University College London, Gower Street, London WC1E 6BT, UK

¹⁶University of California Berkeley, Department of Physics, Berkeley, CA 94720, USA

¹⁷Texas A & M University, Dept. of Physics, College Station TX 77843, USA

¹⁸South Dakota Science and Technology Authority,
Sanford Underground Research Facility, Lead, SD 57754, USA

We describe the development, deployment, and exploitation of a tritium calibration source for the LUX dark matter experiment. The source is useful for calibrating the electron recoil backgrounds over the full volume of the detector, and for characterizing the behavior of the LUX TPC. We report on the LUX electron recoil discrimination factor, the detector threshold, and on the detector physics of liquid xenon at the LUX electric field value of 181 V/cm.

I. Introduction

LUX is a large dual-phase liquid xenon (LXe) time projection chamber (TPC) designed to search for WIMP dark matter with an active target mass of 270 kg. LUX detects both scintillation and charge signals from particle interactions in the LXe. Electron recoil (ER) and nuclear recoil (NR) events are distinguished by the ratio of charge and light signals (S2/S1), and the TPC reconstructs all three coordinates of the event vertex. Results from the first LUX science run (Run 3) were initially reported in Ref. [?]. A

recent re-analysis of the Run 3 data which takes advantage of additional calibrations and an improved understanding of the detector is reported in Ref. [?].

In the WIMP region of interest ($\sim 1 - 8$ keVee), LUX rejects external gamma backgrounds primarily through the passive action of self-shielding, achieving an event rate of XXX mDRU in the fiducial volume. Self-shielding is powerful because gammas in the energy range of interest cannot penetrate to the fiducial volume, while gammas with penetrating power ($> \sim 300$ keV) are unlikely to scatter only once and deposit only a few keV of energy.

While self-shielding makes the detector insensitive to gamma backgrounds, it also presents a challenge for conventional detector calibration techniques for ER events, because external gamma sources such as ^{137}Cs or ^{228}Th are unable to produce a useful rate of single-scatter calibration events in the fiducial volume at low energy. As an alternative, two internal calibration sources that defeat the detectors' self-shielding have been developed and deployed in LUX; the first based upon $^{83\text{m}}\text{Kr}$ [?], and the second based upon tritium (^3H). Unlike external sources, these internal sources are dissolved into the LXe target material, allowing the response of the detector to be studied with a large and spatially uniform sample of events.

$^{83\text{m}}\text{Kr}$ is a source of two internal conversion electrons with energies of 9.4 keVee and 32.1 keVee separated in time by an intermediate state with a half life of 154 ns[?][?]. Because it produces two lines in the energy spectrum, $^{83\text{m}}\text{Kr}$ is suitable for tracking the spatial and time dependence of the S1 and S2 signals. However, because both $^{83\text{m}}\text{Kr}$ electrons are above the energy range of interest for dark matter, and because the S2 signals from the two electrons generally overlap, $^{83\text{m}}\text{Kr}$ is less useful for characterizing the electron recoil (ER) band of the S2/S1 discriminant or for studying the detector threshold.

In this article we report results from the LUX tritium source, which plays a complementary role to the $^{83\text{m}}\text{Kr}$ source. Tritium is a single-beta emitter, with a Q value of 18.6 keVee [?]. Its spectral mean beta energy is 5.6 keVee [?] with a peak at 3.0 keVee. 75% of its beta decays are below 8 keVee [?]. These characteristics make it a nearly ideal source for studying the ER response of the detector in the dark matter energy range. Unlike $^{83\text{m}}\text{Kr}$, tritium is long-lived, with a half-life of 12.3 years[?], so the tritium must be removed from the LXe by purification. In addition, tritium must be introduced into the detector in a manner which will not impair the charge or light collection properties of the detector. This is less of a concern with $^{83\text{m}}\text{Kr}$ since krypton is noble.

We use tritiated methane (CH_3T) as the host molecule to deliver the activity into LUX. Methane has several desirable chemical and physical properties compared to T_2 : first, its diffusion constant (D) times solubility (K) at room temperature is ten times smaller in common LUX materials such as teflon (PTFE) and polyethylene (PE)[?], mitigating the problem of back-diffusion of activity into the liquid xenon after purification; it is chemically inert, so it is not expected to adhere to surfaces (as the T_2 molecule is known to do), and it is consistent with maintaining good

charge transport in liquid xenon. In developing and implementing the tritiated methane source for LUX, we took considerable care to understand and control the removal of the activity from the detector, beginning with a series of demonstration experiments with a small detector. We also attempted to quantify the absorption and back-diffusion of tritiated methane from the plastics used in the LUX detector. The results of these investigations, and our analysis of the risks associated with the tritium injection, are described in the appendix.

An initial tritium dataset of $\sim 7,000$ fiducial events was obtained by LUX in August of 2013, and the results were reported in Ref. [?]. Subsequently, in December 2013, we injected additional activity with a higher initial rate and obtained a fiducial tritium dataset of over 150,000 events. This dataset is used to calibrate the LUX ER band in Ref. [?]. Except where otherwise noted, in this article we report results from the larger December 2013 dataset.

II. Injection and removal of tritiated methane

Two tritiated methane sources with total activities of 0.6 Bq and 200 Bq were prepared for use in LUX. Each source is contained in a 2.25 liter stainless steel bottle and is mixed with 2 atmospheres of LUX-quality purified xenon. The xenon acts as a carrier gas to extract the source from the bottle. The tritiated methane was synthesized for LUX by Moravek Biochemical [?] at a specific activity of 5 milliCurie per millimol.

The injection system is shown in Fig. 1. Only a fraction of the total source bottle activity is extracted during the injection procedure. Activity is extracted from the bottle by allowing the carrier gas to fill one or more expansion volumes consisting of various sections of evacuated tubing. The amount of extracted activity is controlled by selecting an expansion volume of appropriate size. A methane purifier (SAES model MC1-905F) located between the source bottle and the expansion volume ensures that only methane and noble gases are allowed to enter the system. The extracted activity is then injected into the TPC by diverting a small portion of the LUX xenon gas flow through the expansion volumes.

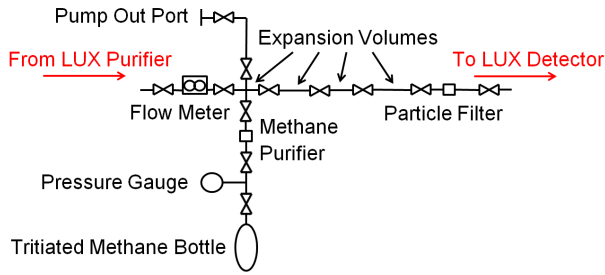


FIG. 1: Plumbing diagram of the tritium injection system for LUX. Tritium is injected downstream of the LUX xenon purifier so that it passes through the detector once prior to being removed. Red arrows indicate the direction of flow.

The tritiated methane appears in the TPC soon after the injection is performed and is removed via the normal action of the LUX xenon purification system, which operates without interruption during the entire procedure. Its centerpiece is a hot zirconium getter (SAES model PS4-MT15-R1) which acts upon gaseous xenon and removes all non-noble species including methane. The xenon gas flow is driven by a diaphragm pump and is facilitated by an efficient two-phase heat exchanger to effect the liquid-gas phase change [?]. The xenon flows in a continuous and perpetual circuit between the TPC and the getter at a rate of 25 SLPM.

Prior to the first injection of tritium activity, we first confirmed that the LUX getter unit was capable of efficient methane removal by injecting ~ 1 ppm (part-per-million) of un-tritiated methane (CH_4) into LUX. As shown in Fig. 2, the CH_4 concentration in the gas was observed over the next several days using a mass spectrometer. The natural methane concentration was observed to decrease exponentially with a time constant of 5.9 ± 0.07 hours. The one-pass efficiency of the getter for methane was measured to be 97% under the LUX flow and temperature conditions by sampling the gas before and after the getter.

On August 8, 2013, an initial injection of 20 mBq of tritiated methane was performed, followed five days later by an injection of 800 mBq. The count rate of fiducial single-scatter events with S1 less than 150 phe during this time period is shown as a function of time in Fig. 3. The tritium activity is clearly observed. For both injections the activity was removed with a six-hour exponential time constant similar to that observed in the CH_4 injection. It is interesting that the purification time constant is con-

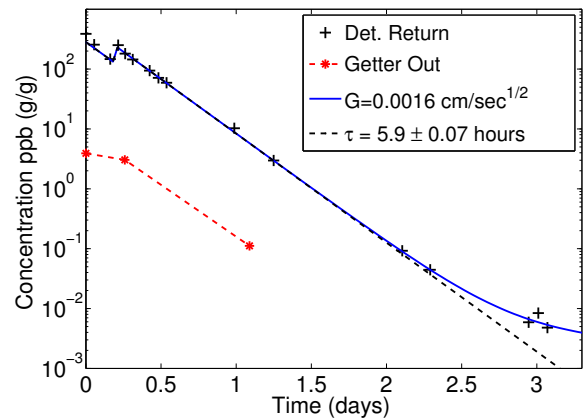


FIG. 2: Removal of natural methane observed by the integrated xenon sampling system prior to the tritiated methane injections. The red points indicate measurements at the getter outlet, we find a 97% one pass removal efficiency at a flow rate of 25 SLPM. The blue curve shows the improved upper limit on the effect of outgassing from the plastics. The black dashed lines shows the exponential fit to the natural methane removal from the xenon with a time constant of 5.9 ± 0.07 hours. 5×10^{-3} ppb (g/g) is the limit of detection for methane.

siderably shorter than the naive volume turn-over time of LUX (about 41 hours for 370 kg of xenon at a gas flow rate of 25 SLPM). The origin of short purification time remains under investigation.

The location of a the tritium events from the first injection is shown in Fig. 4. As expected the events are uniform within the detector volume.

III. Results

In December of 2013 a total of 10 Bq of tritiated methane was injected into LUX and removed. A total 325,000 events were observed in the active volume of LUX. 140,000 events were collected in the fiducial volume at the nominal LUX electric field of 170 V/cm, while 4,500 fiducial events were collected in a special run at a reduced field of 100 V/cm. The S1 and S2 signals are corrected for spatial effects such as the light collection efficiency and the free electron lifetime with ^83mKr data as described in [?

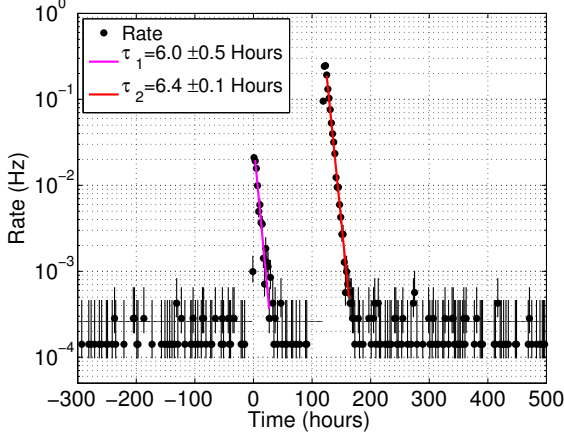


FIG. 3: Left: Rate of single scatter events with S1 below 150 Phe in the fiducial volume during the August 2013 tritium injections. 150 Phe in S1 is about 18.6 keVee, the endpoint of the tritium beta spectrum. The magenta and red curves are exponential fits to the activity vs time.

].

We interpret the data in terms of the combined energy model [?], where the total energy of an event is directly proportional to the number of quanta produced (electrons plus scintillation photons):

$$E_{total} = W \cdot (n_\gamma + n_e)$$

We use a W value of 13.7 eV/quanta [?]. In LUX n_γ and n_e are proportional to the S1 and S2 signals, with gain factors g_1 and g_2 :

$$E_{total} = W \cdot \left(\frac{S1}{g_1} + \frac{S2}{g_2} \right)$$

where S1 and S2 have units of phe and g_1 and g_2 have units of phe per quanta. g_1 may be interpreted as the light collection efficiency times the average quantum efficiency of the PMT arrays, while g_2 is the electron extraction efficiency at the liquid-gas surface times the secondary scintillation gain factor and the PTM quantum efficiency. g_1 and g_2 are measured with line source data in LUX as described in Ref. [? ?]. We find values of $g_1 = 0.115 \pm 0.003$ and $g_2 = 5.39 \pm 0.522$.

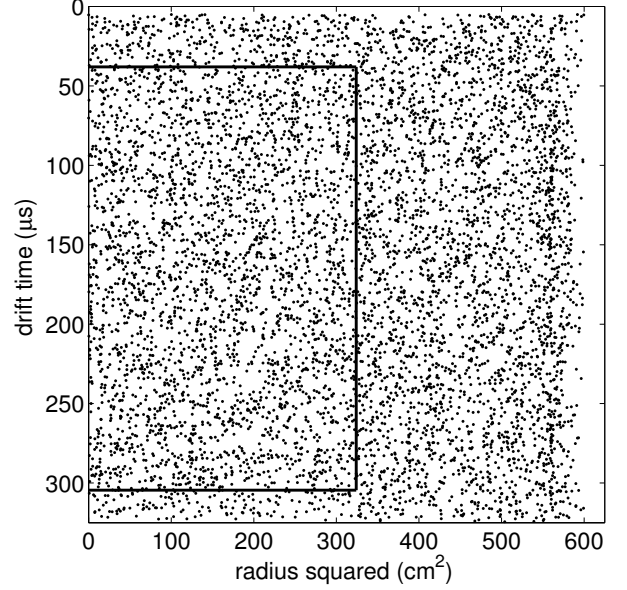


FIG. 4: The location of events in drift time vs. detector radius squared for the first tritium injection. The drift time is a proxy for the z coordinate of the event. The solid black line represents the fiducial volume used in [?].

A scatter plot of n_e vs n_γ for the tritium data at 170 V/cm is shown in Fig. 5, along with the projected histograms on each axis. The tritium energy spectrum, obtained by projecting the data along the lines of constant energy, is shown in Fig. 6. The data is compared to several models: a pure tritium spectrum, with no detector effects; a spectrum simulated with LUXsim, and a tritium spectrum with a simple energy smearing factor of $\sigma_E = XXXX$ applied. The ratio of the data to the smeared tritium spectrum is shown in Fig. 7, along with a fit to an error function. The ratio shows that the data is modeled well by the smeared tritium spectrum, and the effective low energy threshold of 50% efficiency is found to be 1.04 ± 0.016 keV.

The mean light yield and charge yield of ER events in LUX are obtained by dividing the mean light and charge signals by the combined energy in each energy bin. The result is shown for 170 V/cm in Fig. 8. For these plots a small correction has been applied to the data to account for smearing of tritium events across energy bins due to the detector's resolution [?].

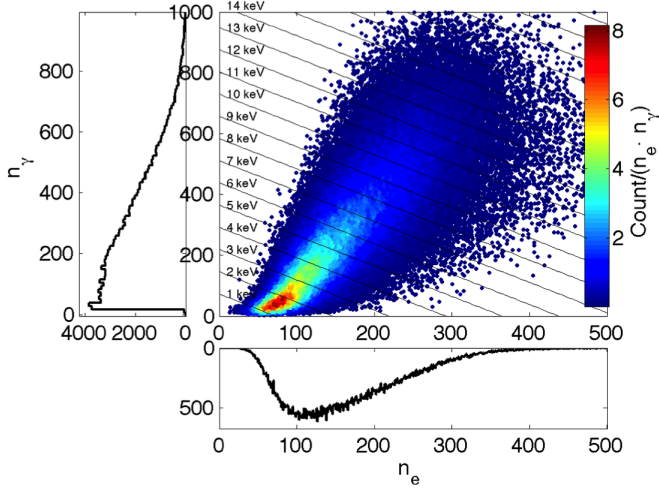


FIG. 5: Scatter plot of n_e vs n_γ for 115,000 fiducial tritium events at 170 V/cm. Lines of constant energy are indicated assuming a W value of 13.7 eV/quanta. The data is projected into n_e and n_γ histograms on each axis.

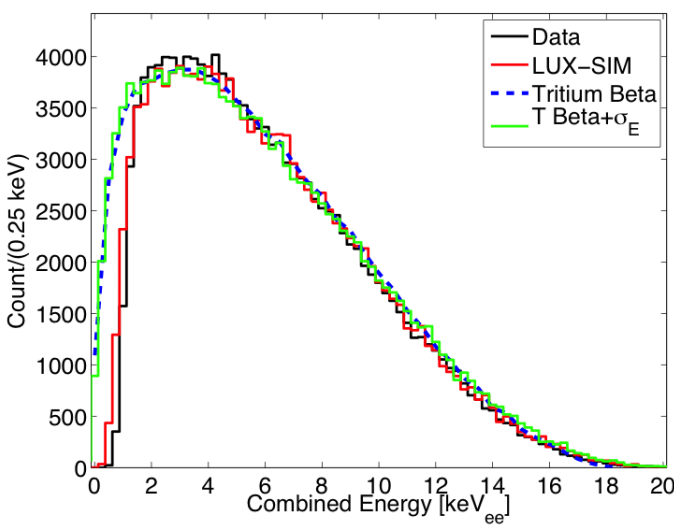


FIG. 6: The tritium energy spectrum measured by LUX with the combined energy model (black) compared to several theory models: a pure tritium spectrum (dashed blue), LUXsim (red) and a tritium spectrum with a simple energy smearing of $\sigma_E = XXXX$ applied.

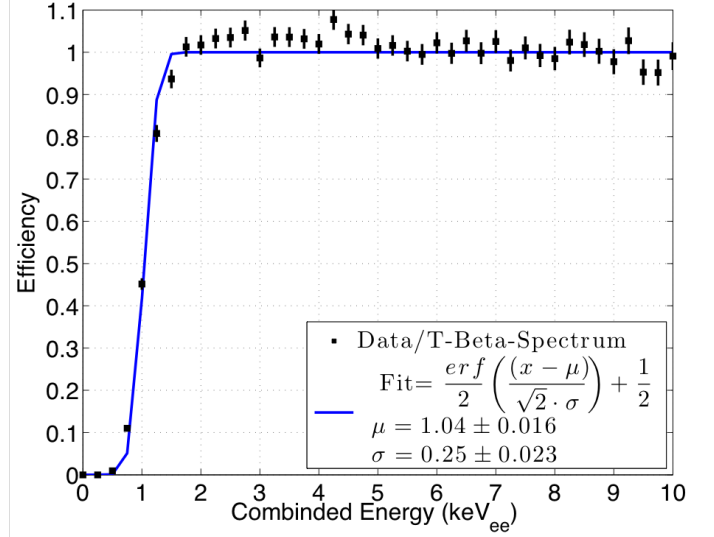


FIG. 7: ER threshold measured by comparing the measured energy spectrum to the smeared tritium spectrum. A fit to an error function is shown.

As shown in Fig. 8, the light yield is observed to drop rapidly between 1 and 6 keV, and then become mostly energy independent over the remainder of the tritium spectrum. The charge yield exhibits the reverse behavior, as expected from the combined energy model. These effects can also be illustrated by plotting the total number of quanta as a function of energy, as shown in Fig. 9 for tritium events between 1 and 8 keV. Also shown in Fig. 9 are the total number of quanta assuming a W value of 13.7 eV/quanta (black), and the primary number of ions (violet) and excitons (cyan) prior to recombination assuming an initial exciton-to-ion ratio of 0.2 [?]. In a model where the number of observed electrons differs from the number of primary ions due solely to recombination, we can interpret the charge yield data as a measure the recombination fraction at each energy. Accordingly,

$$r = \frac{\frac{n_\gamma}{n_e} - \alpha}{\frac{n_\gamma}{n_e} + 1}$$

where r is the recombination fraction and α is the assumed value of the primary exciton-to-ion ratio. Taking $\alpha = 0.2$, we find the recombination fraction as a function of energy as shown in Fig. 11. Here the falling charge yield and

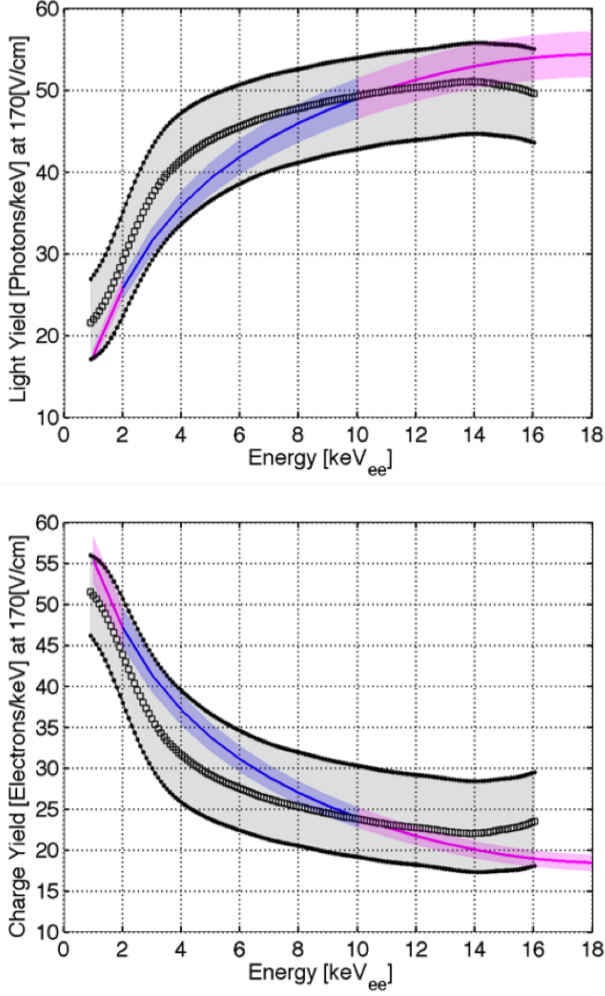


FIG. 8: The light yield and charge yield of ER events in LUX at 170 V/cm compared to NEST v0.98 (2013). The grey bands indicate the systematic errors on g_1 and g_2 , which are fully correlated across all energy bins. g_1 is anti-correlated with g_2 , such that an increase in the charge yield within the grey band must be compensated by an equivalent decrease in the light yield. Upper: Light yield at 170 V/cm. Lower: the charge yield at 170 V/cm.

rising light yield between 1 and 6 keV is interpreted as a rapid rise in the recombination fraction.

We obtain the LUX ER band by plotting $\log(S_2/S_1)$ vs S_1 as shown in Fig. ????

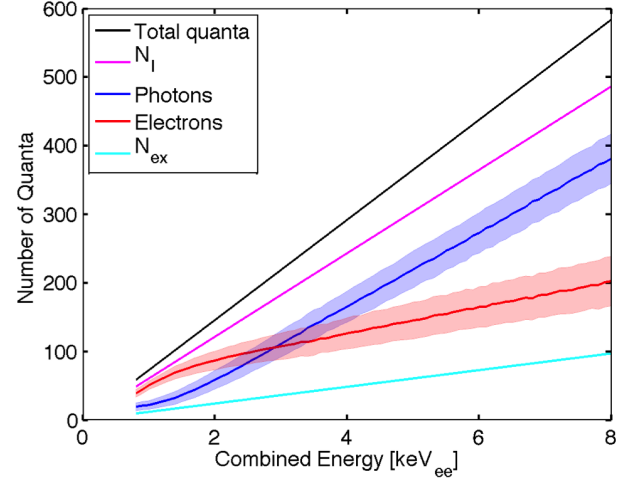


FIG. 9: The mean number of electrons (red) and scintillation photons (blue) produced in LUX at 170 V/cm as a function of energy. The bands indicate the correlated systematic errors on g_1 and g_2 . Also shown are the total number of quanta, primary ions, and primary excitons, assuming an exciton to ion ratio of 0.2.

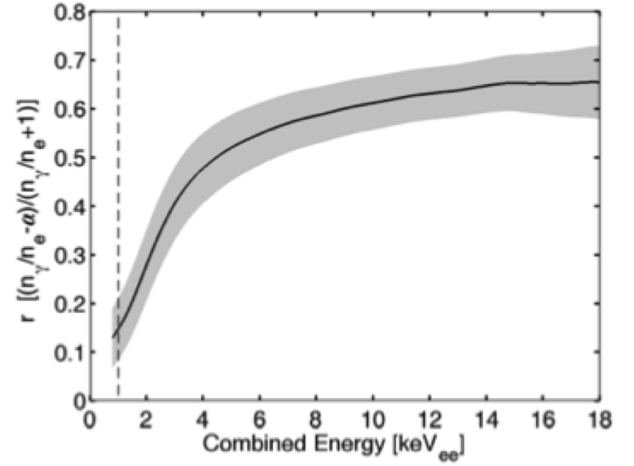


FIG. 10: Recombination fraction of ER events at 170 V/cm, assuming an exciton-to-ion ratio of 0.2.

The electronic recoil band in the fiducial volume of the LUX detector was calibrated to unprecedented accuracy

using the tritium source. Figure 12 shows the tritium calibration data with fits to the mean of the ER band along with the 10-90% confidence bounds ($\pm 1.28\sigma$), at a drift field of 180 V/cm. The values of the leakage fraction at 50% NR acceptance per each 1 Phe bin in S1 are shown in 13. The nuclear recoil band, in red, is defined by the NEST model along with AmBe and ^{252}Cf calibrations. The amount of methane injected to perform the calibration was less than 1 part-per-trillion ($< 10^{-12}$) far to small to cause degradation in electron lifetime or quench xenon scintillation [?]. We have also independently verified the null impact on electron lifetime and light yield by performing a tritiated methane while taking $^{83\text{m}}\text{Kr}$ calibration data [cite, thesis].

WIMPs primarily interact with the atomic nuclei of xenon atoms in LUX resulting in nuclear recoils whereas the vast majority of residual radioactivity within the detector are gammas which result in electronic recoils. Thus, knowing the separation of the ER from the NR band allows for a measure of the background rejection figure of merit for a liquid xenon experiment. We define the background rejection figure of merit as leakage fraction, reported here as the fraction of ER events that leak into the lower half of the NR band. Over 115,000 tritium decays were used for the ER band calibration, between 1-50 Phe in S1 (1-8 keV_{ee}), and were found using standard WIMP search cuts within the fiducial volume. Figure 13 shows the leakage fraction per 1 Phe bins of S1. The mean leakage fraction in the region used for the LUX 2013 PRL results, between 1-30 Phe (1-5 keV_{ee}) in the fiducial, was found to be $0.42\% \pm 0.02\%$, see Figure 13. Figure 14 shows the reconstructed energy spectrum for those tritium events in the fiducial volume of the detector (black) along with the tritium spectrum from NEST modeling (blue) and an ideal tritium spectrum (magenta). The reconstructed energy matches the tritium beta spectrum well from 1 to 18 keV_{ee} . The calibration data was acquired in a 40 hour time window in which less than three out of 115,000 events are expected to be non tritium [?], this implies a near perfect data purity for the calibration. Nearly every point (99.997%) show in figure 12 and the histogram of 14 is the result of a tritium beta decay in the fiducial volume of the LUX detector.

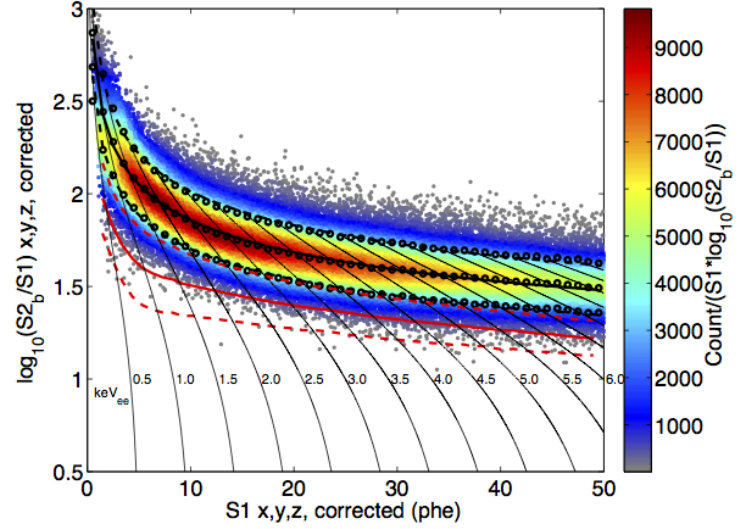


FIG. 11: Discrimination vs. S1 using over 115,000 tritium beta decays between 1 and 50 Phe in S1 (about 1 – 8 keV_{ee}). On average from 1 to 30 Phe the discrimination is 99.58%, defined by the fraction of events of events below the mean of the nuclear recoil band. The red band represents the NEST nuclear recoil band (version 0.98) vetted with an AmBe, ^{252}Cf and DD neutron generator calibration.

1. Threshold Determination

The tritiated methane calibration source provides beta decays with energies down to 0.1 keV_{ee} allowing for an independent measure the LUX detector's threshold. The limitation for detecting a single scatter WIMP like event with PMTs is the S1 (primary scintillation) signal, being more than an order of magnitude less than the S2 signal. The S1 threshold could be measured by comparing the NEST model, assuming perfect detector resolution, to the observed tritium beta spectrum from 0.1-10 keV_{ee} . The threshold determined by comparing the tritium data to NEST is in good agreement with all other methods used for determining the threshold in the LUX detector, figure 15.

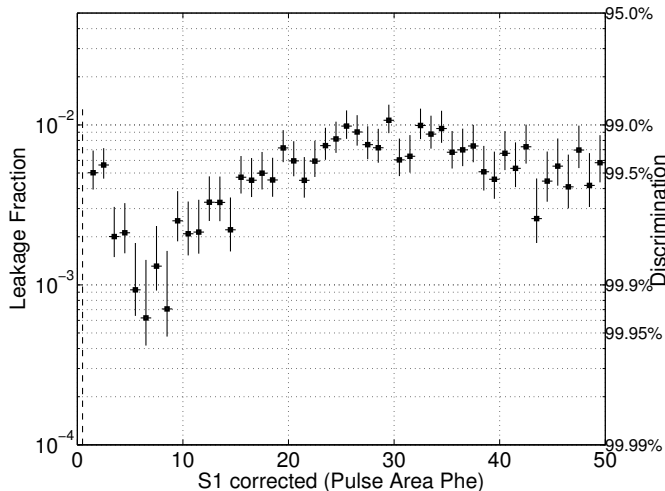


FIG. 12: Discrimination vs. S1 using over 115,000 tritium beta decays between 1 and 50 Phe in S1 (about $1 - 8\text{keV}_{ee}$). On average from 1 to 30 Phe the discrimination is 99.58%, defined by the fraction of events of events below the mean of the nuclear recoil band. The red band represents the NEST nuclear recoil band (version 4c) vetted with an AmBe, ^{252}Cf and DD neutron generator calibration.

IV. Additional Calibrations with Tritium

In this paper we have described the development and use of a tritiated methane calibration source for large scale xenon detectors. The primary application of the tritiated methane calibration source is to characterize the ER band and measure discrimination from electronic and nuclear recoils. However, much more fundamental xenon physics can be probed with the tritium calibration source. With higher statistics the discrimination can be measured in finer bins of energy or S1 Phe (figure 13) along with the Gaussianity of the ER band. The $\log(S2/S1)$ has been assumed to have Gaussian behavior in past experiments, never before has there been an ER calibration with such high data purity in the WIMP search region to observe potential non-Gaussian behavior. The largest tritium calibration in LUX detector's fiducial region produced 115,000 tritium beta decays with only three being non tritium events. The tritium calibration can also used to calculate the light yield, charge yield and recombination fluctuation

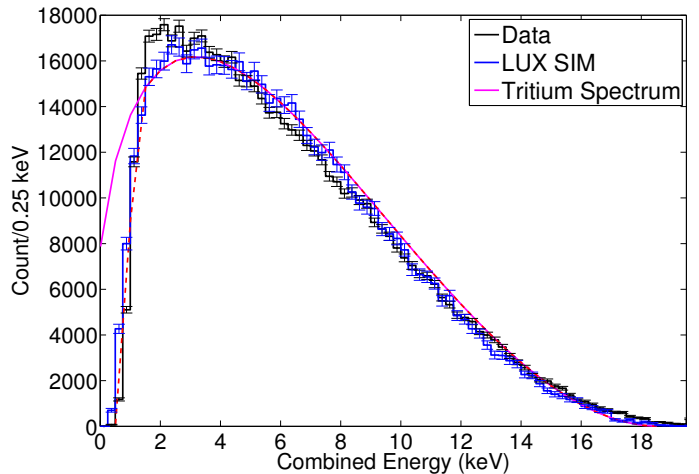


FIG. 13: Energy histogram of tritium events. The black histogram represents the data, in blue is the tritium spectrum produced with LUX SIM based on NEST. The magenta curve shows the true tritium beta spectrum without smearing due to finite detector resolution, the dashed line indicates the true tritium spectrum convolved with the threshold

over the range from 1 to 18 KeV_{ee} . The current data taken with the LUX detector has allowed for the vetting of the NEST model down to 1 keV_{ee} for the first time. Finally, tritium provides a low energy uniformly distributed source making it ideal for determining the fiducial volume of a detector and calibrating position reconstruction algorithms for low energy events.

V. Summary

We have presented our new technique for injecting and removing CH_3T as an internal calibration source in detectors which utilize liquid and gas phase noble gases. We discussed the assembly of our CH_3T calibration system, motivated by gas and liquid phase R&D experiments at the University of Maryland. We have used data from the LUX detector to show that our system can safely inject CH_3T for the purpose of internal calibration.

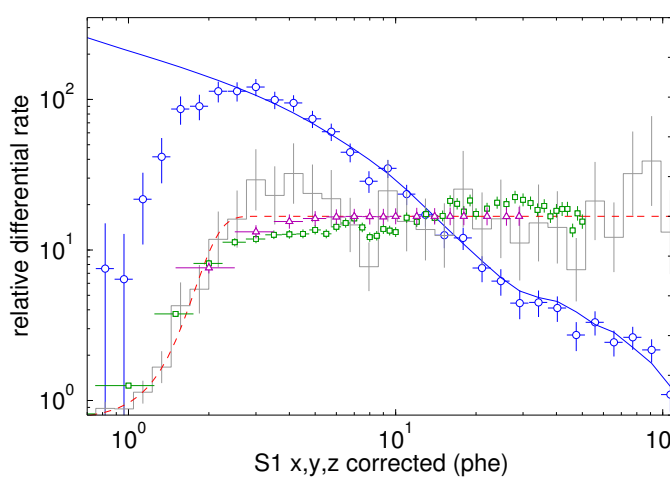


FIG. 14: Comparison of AmBe data (blue circles) with NEST simulations (blue line), showing excellent agreement above the 2 phe threshold (left axis). The gray histogram and fitted dashed red line show the relative efficiency for detection of nuclear recoils from AmBe data (right axis). Overlaid are the ER detection efficiency from tritium data (green squares), applied to the ER background model in the profile likelihood analysis, and the efficiency from full detector NR simulations treated as real data in terms of the digitized MC-truth S1 phe (purple triangles), applied to the WIMP signal model. The efficiency calculation here does not include S1 or S2 area thresholds.

VI. Development of the Calibration Source

In developing and deploying the source, our purification goal was that any residual activity that remained due to back-diffusion from plastics or from inefficient purification should be no more than $0.33 \mu\text{Bq}$, which is 5% of the LUX ER background rate design goal for a 30,000 kg-days exposure. We desired to collect a LUX calibration dataset of $\sim 15,000$ tritium events, roughly a factor of 100 larger than the number of expected ER background events in LUX [?].

In addition to providing a direct measure of the removal rate of methane from LUX, the natural methane injection allowed a stronger and more direct limit to be placed on the outgassing from the plastics. As seen in figure ??, the highest value allowed for the outgassing constant is

$0.0016 \text{ cm/day}^{1/2}$, which is in agreement with the lower limit discussed in section 2. We call this an upper limit because the apparent elbow observed in the data occurs at the sensitivity limit of the sampling system. With the measurement of both the outgassing constant, and the removal rate of methane, it is now possible to place strong limits on the time cost of performing a tritiated methane calibration, as shown in figure 16.

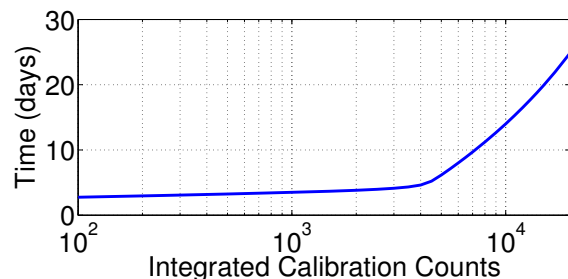


FIG. 15: Shown above is the time required to allow the tritium activity to fall to $< 5\%$ of the nominal LUX background, calculated using the purification rate and outgassing constant measured during the natural methane injection.

1. Tritiated Methane Removal

The removal efficiency of zirconium getters for methane in xenon had previously been studied at the University of Maryland. It was found that greater than 99.99% of natural methane can be removed in a single pass through a zirconium getter. [?] Tritiated methane is chemically identical to natural methane, so it follows that similar removal efficiencies should be expected for CH_3T . To verify this a small scale tritiated methane injection system was integrated into a liquid xenon system at the University of Maryland. This system used a SAES MC1-905F methane purifier placed in series immediately after the CH_3T source bottle to prevent non-methane species of tritium from entering the plumbing. Over 68,000 Bq of observed CH_3T activity was injected into this small scale system and a removal efficiency of over 99.99% for tritiated methane in xenon was confirmed.

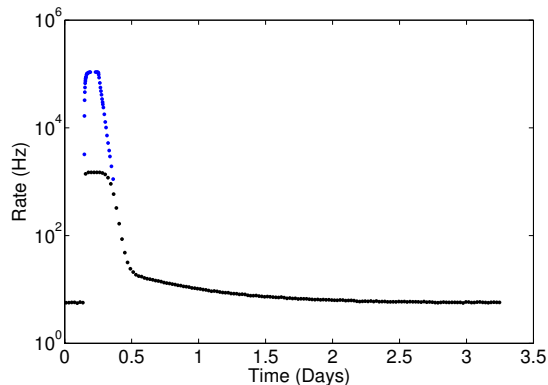


FIG. 16: A time histogram of the event rate during a tritium injection into our small scale detector. The event rate greatly exceeded the limits of our ADC (black data points), so a analog scalar was used to count the true event rate (blue data points).

2. Out Gassing of Tritiated Methane from Plastics

An accurate model of a tritiated methane injection into LUX must account for out gassing of CH_3T from plastics such as polyethylene and teflon. Using data from the liquid xenon experiments at the University of Maryland we numerically modeled the purification and residual diffusion of CH_3T in the detector. Using Duhamel's principle, an integral solution to Fick's second law on a half-infinite line can be found to be

$$\phi(x, t) = KC_{out} - \int_0^t \text{erf}\left(\frac{x}{\sqrt{4D(t-\tau)}}\right) KC_{out}(\tau) d\tau - KC_{out}(0) \text{erf}\left(\frac{x}{\sqrt{4Dt}}\right),$$

where K is the solubility of the material, D is the diffusion constant, and C_{out} is the concentration at the surface of the material. For the out gassing process we are only able to detect the flux of material out of the plastic. This is given by Fick's first law evaluated at $x = 0$,

$$J_{out}(t) = -K\sqrt{\frac{D}{\pi}} \left(\int_0^t \frac{C_{out}(\tau)}{\sqrt{t-\tau}} d\tau + \frac{C_{out}(t)}{\sqrt{t}} \right),$$

where the sign has been flipped since the flux of material is outward. We see that it is no longer possible to evaluate K and D separately, since the diffusion in and out of the plastic is completely determined by the time-dependent con-

centration outside of the plastic. To simplify our model, we define a new constant

$$G = K\sqrt{\frac{D}{\pi}}.$$

By fitting the integral of the flux out of the plastic over time to out gassing data collected in Maryland's liquid xenon system we constrain $G \leq 0.0075 \frac{\text{cm}}{\sqrt{\text{day}}}$.

With a constraint on G taken from the analytic solution to Fick's second law, we turn to numerical simulation to answer the question of how much initial CH_3T activity to inject into LUX to meet our calibration conditions. Several assumptions are made to simplify the numerical model. First, we approximate the diffusion into plastic as being a one dimensional process. Since the plastic in our detector at Maryland and in LUX can be approximated by a cylindrical shell, there is no dependence on the azimuthal or z coordinates. Since r is large compared to the thickness of the plastic shell, $\frac{\delta^2 \phi}{\delta r^2} \gg \frac{1}{r} \frac{\delta \phi}{\delta r}$, so Fick's laws in a one dimensional approximation become

$$J = -D \frac{\delta \phi}{\delta r} \vec{r}$$

$$\frac{\delta \phi}{\delta t} = D \frac{\delta^2 \phi}{\delta r^2}.$$

We assume the concentration of CH_3T in LUX is uniform throughout its volume, since the design of LUX creates currents which stir the liquid xenon. With perfect mixing the effect of the purifier can be modeled by adding an exponential time dependence to the outer volume. The time constant of this decay has an upper limit equal to the time it takes xenon to recirculate through the LUX detector, although in reality the mass transport from diffusion in the liquid and gaseous xenon decreases this time constant.

We use a simple implementation of the first order Euler method for our numerical simulations. The diffusion is simulated by setting the concentration at the boundary of the piece equal to KC_{out} , where C_{out} is the concentration of CH_3T in the xenon. This concentration is dependent on time according to

$$\frac{\delta C_{out}}{\delta t} = J_{out} \frac{A_{plastic}}{V_{xenon}} - \frac{C_{out}}{\tau},$$

where $A_{plastic}$ is the surface area of the plastic cylinder, V_{xenon} is the total volume of xenon in the fiducial region,

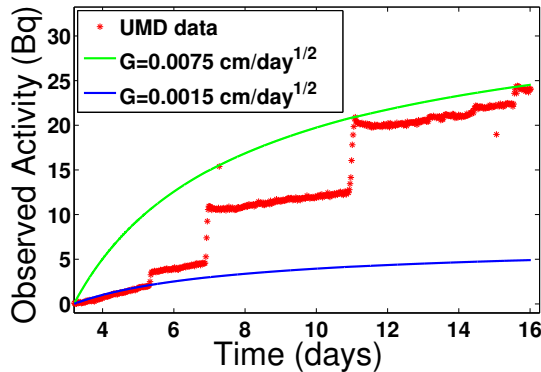


FIG. 17: This plot shows the tritium activity observed after an injection into the small scale detector at Maryland. There were several polyethylene panels placed in the liquid xenon during this injection, and after about 3.5 days, the getter was put into bypass mode and the activity began to rise. The blue curve shows the upper limit of G which accounts for the steps seen in the data (the red points). The green curve, which shows the lower limit, assumes that these steps are not due to the outgassing from the PE panels and only fits to data before the first jump.

and τ is the characteristic removal time of methane from LUX (with perfect mixing and purification efficiency, this will be identical to the turnover time of xenon in LUX, but purifier inefficiencies and Henry's Law solubilities can have a significant effect on this value). The first term on the right of this equation models out gassing of CH_3T from the plastic cylinder, while the second term models removal of CH_3T through purification. Using the first order Euler method, we arrive at an expression for C_{out} given by

$$C_{j+1} = C_j + \Delta t \left[(J_{1,j} - J_{N_x,j}) \frac{A_{plastic}}{V_{xenon}} - \frac{C_j}{\tau} \right].$$

The initial concentration is defined by dividing the desired injection activity by the volume of the fiducial region. We choose $D = 2.3 \times 10^{-9} \frac{\text{cm}^2}{\text{sec}}$ so that the half-infinite boundary conditions in our diffusion model is valid, and combine this with our allowed range of values for G to extract a value for K . We use this model to predict the total number of calibration events as well as the time required to return to $<5\%$ of the nominal background rate for any CH_3T injection into LUX.

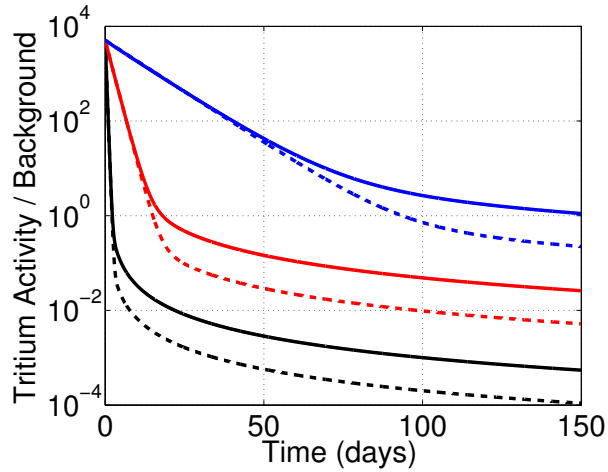


FIG. 18: Displayed are the results of simulated 0.1 Bq injections of tritiated methane into LUX. The dashed curves assume the lower limit of G ($0.0015 \text{ cm/day}^{1/2}$), while the solid curves assume the upper limit of G ($0.0075 \text{ cm/day}^{1/2}$). The black curves assume a characteristic removal time of 0.25 days, the black curves assume 1.7 days, and the blue curves assume 10 days.